IEEE Robotics and Automation Letters (RAL) paper presented at
2024 IEEE/RSJ International Conference on Intelligent Robots and Systems (IROS)
October 14-18, 2024. Abu Dhabi, UAE

Optical-Waveguide Based 3-Axial Tactile Sensor for Minimally Invasive Surgical Instruments

Yue Li, Wenlong Gaozhang, Jian Hu, Danqian Cao, Prokar Dasgupta and Hongbin Liu

***Abstract*— Force feedback is of importance in Minimally Invasive Surgery (MIS) as it reduces surgical risks and enhances surgical safety. However, equipping force sensing to the tip of surgical instruments presents challenges due to their diminutive dimensions and often curved shapes. To address this issue, a novel and compact optical-based 3-Axial force sensor used for the surgical forceps is proposed. Based on the extent of disruption to the total internal reflection (TIR), the magnitude and the direction of the force can be detected by measuring the light intensity patterns from three intersecting channels. The calibration experiments validate the capability of the proposed sensor to accurately measure forces within the range of 0 to 3N, achieving an average measurement error of 0.089N. Subsequently, the sensor, along with the detection circuit, are integrated onto a surgical forcep, and verification experiments are conducted. The results indicate that the proposed sensor can provide effective 3-Axial force sensing during the surgical process such as grasping, manipulation, and pulling. The characteristics of compact size, high precision, and integrability of the sensor make it highly promising for providing force feedback in MIS.**

***Index Terms*— Force and Tactile Sensing, Haptics and Haptic Interfaces, Flexible Robotics.**

I. Introduction

MINIMALLY invasive surgery (MIS) represents a surgical modality conducted using minimally sized incisions [1]. MIS demonstrates notable merits including reduced tissue damage, diminished discomfort, and expedited convalescence [2], [3]. However, from a medical standpoint, the absence of haptic feedback during the process of MIS poses a significant obstacle [2], [4], [5]. The incorporation of force feedback presents a more dependable means of mitigating the risk of inadvertent application of excessive force by surgeons, which can prevent tissue damage [6], [7]. Furthermore, the inclusion of grasping force feedback aids in averting tissue slippage, consequently improving the time efficiency of MIS [7]. Hence, there exists a vital imperative to advance the development of sensorized MIS instruments that have the capacity to discern the external forces.

With regard to the properties of MIS, tactile sensors should meet the requirements of high sensitivity, compact integration, cost-effectiveness, miniaturization and multi-dimension force identification. Recently, there has been an increasing focus on the integration of force sensors on the minimally surgical instruments [8]. The advancements in sensor development are primarily focused on achieving the sensor's multi-dimensional capabilities while ensuring compact integration. However, there is a trade-off between miniaturization and functionality due to methods for force measurement are based on electrical force sensing technologies [9], [10], [11], including piezoresistive [12], [13], piezoelectric [14], [15], [16], and capacitive sensors [17], [18], [19]. Although electrical based sensors offer high sensitivity and accuracy, their adoption in MIS tools is limited by the wiring complexity while the weak connections between wires may impair the sensing performance with the moving of instruments.

Compared with the conventional electrical force sensing, optical-based tactile sensing has unique advantages of simplified wiring, flexibility, and biocompatibility [7], [20]. Moreover, its compatibility with sterilization processes, resistance to various chemical interferences, and immunity to electromagnetic interference make it a highly promising candidate for MIS [21], [22], [23], [24]. An optical-based sensor operates on the principle of transmitting light through an input to a detector, where the characteristics of the intensity, wavelength, amplitude, and phase, can response to change accordingly [25]. Xie et al. [22] proposed an optical tactile array probe head consists of 14 tactile sensing elements positioned at 2.5-mm spacing with a diameter of 14 mm for the distributed normal force detection. Similarly, Back et al. [26] introduced an ellipse-shaped probe with 16 sensing units, which allowed for the visualization of pressure maps within a force range of 0-1.622 N and the error was 3%. However, miniaturization is also a challenge that needs to be addressed for MIS applications. In the research conducted by Tang et al, an optical nanofibers tactile sensor with a resolution of 0.031 mN was proposed for hardness discrimination [27]. Optical fiber Bragg gratings (FBGs) were employed in Lim et al. [28], He et al. [29] and Li et al. [30]'s work to provide the force feedback

Manuscript received: August 28th, 2023; Revised: November 12th, 2023; Accepted: December, 7th, 2023.

This paper was recommended for publication by Editor Jessica Burgner Kahrs upon evaluation of the Associate Editor and Reviewers' comments.

This work was supported by InnoHK program. The work of Yue Li was supported by China Scholarship Council under CSC NO. 202006280025.

Yue Li, Danqian Cao, Hongbin Liu are with the School of Biomedical Engineering & Imaging Sciences, King's college London, London, SE1 7EH, UK (e-mail: yue.3.li@kcl.ac.uk; danqian.cao@kcl.ac.uk; hongbin.liu@kcl.ac.uk).

Wenlong Gaozhang is the School of Mechanical Engineering, University college London, London, WC1E 6BT, UK (e-mail: ucemaoz@ucl.ac.uk).

Jian Hu, Hongbin Liu are with Chinese Academy of Sciences, Institute of Automation (CASIA), Beijing, China and the Centre of AI and Robotics (CAIR), Hong Kong Institute of Science & Innovation, Chinese Academy of Sciences, Hong Kong, China. (e-mail: hujian@ia.ac.cn; liuhongbin@ia.ac.cn).

Prokar Dasgupta is with MRC Centre for Transplantation, NIHR Biomedical Research Centre, King's College London, and Guy's and St. Thomas' NHS Foundation Trust, Urology, London, UK (e-mail: prokar.dasgupta@kcl.ac.uk).

Digital Object Identifier (DOI): see top of this page.

while the resolution can reach up to 11mN, 0.4mN, 0.93mN. However, the current optical-based sensor often come with higher-cost demodulation equipment, requiring simplifying the system in a more cost-effective way [7].

In our previous research, we proposed optical-based tactile sensors that utilizing the principle of total internal reflection (TIR) of waveguides to detect the magnitude of normal force by establishing a relationship between applied force and the output light intensity [21],[31],[32]. Furthermore, in the work of [33], we further optimized the sensor structure to differentiate between normal and shear forces from different directions through the design of a cross-symmetric structure. However, the previous studies employed a mounted LED as the light source and utilized a linear camera for measuring the output light intensity, which present significant challenges for practical applications because of its expensive cost and non-integrability. Additionally, the size of the previous sensor exceeded the constraints for integration onto MIS forceps typically used in surgical procedures.

To address these limitations, this paper focus on further optimizing the sensor design to achieve multi-dimensional sensing and integration specifically for MIS applications. Given that surgical forceps used in MIS typically exhibit an asymmetric structure, we designed a customized sensor to enable sensing of both normal and shear forces, suitable for curved surfaces for MIS forceps. Moreover, to differentiate forces from different directions, we proposed a novel waveguide pattern which reduces the number of channels, resulting in a more compact sensor size compared to previous sensor. To achieve uniform deformation of the sensing area, the different shapes of the force indenter were studied concerning the contact deformation of soft-rigid interfaces. Furthermore, a compact and highly integrated light source and light intensity detection module were developed that then be installed at the tip of the forceps to verify the feasibility of the sensor for using in MIS.

II. Sensor Concepts

A. Sensor Design

A prototype of the laparoscopic curved dissecting forceps incorporating the tactile sensor was designed in this paper, as shown in Fig. 1. It comprises a grasping joint, tool shaft, joint actuation unit, and sensorized forceps.

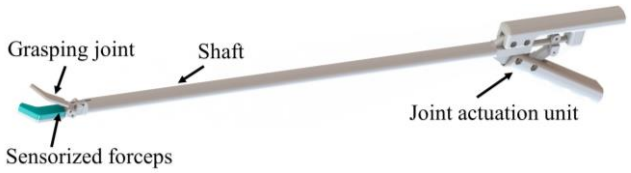

Fig. 1. Prototype of surgical forceps incorporating the tactile sensor.

Based on it, we proposed a tactile sensor with a width range of 4-8mm and a length of 23mm, as shown in Fig. 2. Three optical waveguides with a cross-sectional dimension of 0.7mm×0.7mm intersect each other with 90 degrees are designed for efficient light propagation. A square soft tactile element (Tactel) is formed by the intersection of three channels with a side length of 2.6mm, and it is designed to perceive and discern the magnitude and direction of external force. Firstly, the light is emitted from LED and propagates towards the input of the waveguide. Subsequently, the light is split into three channels and then the detectors employed at the end of each channel is used to measure the changing of the light intensity.

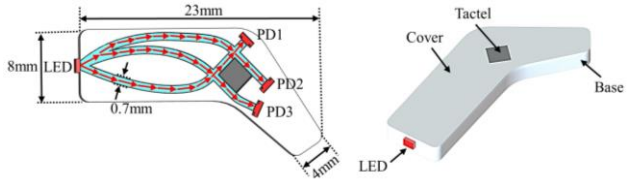

Fig. 2. The layout of the proposed sensor. (a) The optical path of the waveguide. (b) the proposed sensor.

For the waveguides, Clear Flex 30 was chosen as the core material with a refractive index of 1.47[25]. It is noteworthy that PTFE material with a refractive index of 1.38 was utilized as both the cladding material and the base of the sensor [34]. Under initial conditions, light propagation of the waveguides follows the principle of total internal reflection (TIR) when the angle of incidence θc is larger than the critical angle [21]. The critical angle ϕ was calculated by (1), which was 69.84 degrees in this paper

$$\phi = \arcsin(\frac{n_2}{n_1}) \tag{1}$$

where n_1 and n_2 are the refractive index of the core and the cladding.

B. Working Principle

In terms of normal force sensing, the application of force on the tactel aligned with the negative z-axis, induces compression and consequent expansion along the three lateral sides, leading to the disruption of total internal reflection (TIR) of three channels. Consequently, there is a direct correspondence between normal force and light losses observed across all three channels, as shown in Table 1.

As for shear force sensing, the consequent changing light intensity from three waveguides exhibit distinct variations because of the asymmetric deformation of the sensing area. Table 1 presents the specific and distinct corresponding channels when shear forces emanate from different directions. Notably, when the shear force is directed along the positive y-axis, channels 1 and 2 experience significant compression, resulting in a more obvious decrease of their light intensities compared to channel 3. In contrast, when the shear force is applied along the negative y-axis, it leading to a significant decline of channel 3 as the force increases. Similarly, when the shear force is applied along the positive x-axis, channel 2 displays the primary response, whereas channels 1 and 3 are the corresponding channels when the force is in the opposite direction.

It is noteworthy that one side of the tactel is directly connected with the rigid base. When a force is applied in this specific direction, it induces deformations of channels 2 and 3 instead of in alignment with the force vector, consequently leading to the decreasing output of channels 2 and 3 correspondingly. Based on this principle, we can effectively obtain the measurements of 3-Axial force magnitude and direction by the combinations of light intensity variations of the outputs from three waveguides.

TABLE I. WORKING PRINCIPLE OF THE PROPSOED SENSOR

Force Direction	Force Vector (x,y,z)	Deformation result	Corresponding Channel		
			1	*2*	*3*
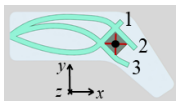	(0,0,-1)	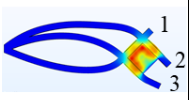	√	√	√
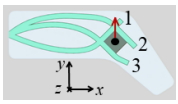	(0,1,-1)	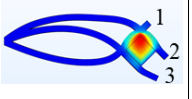	√	√	—
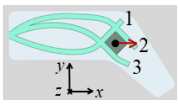	(1,0,-1)	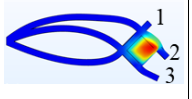	—	√	—
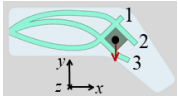	(0,-1,-1)	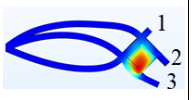	—	—	√
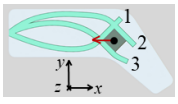	(-1,0,-1)	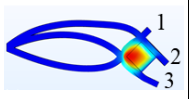	√	—	√
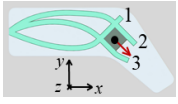	(1,-1,-1)	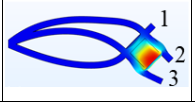	—	√	√

√. Corresponding Channels —. Uncorresponding Channels

C. *Fabrication Process*

The proposed sensor was manufactured by molding into computer numerical control (CNC) fabricated molds, including the PTFE base mold, cover base mold, and metal L-shaped fixed mold, as shown in Fig. 3. Initially, all the molds were machined and followed by a ten-minute ultrasonic cleaning to eliminate surface impurities. Subsequently, the sensor cover and base were tightly aligned and vertically positioned within the fixture. The fixture, adjacent to the cover (Fig. 3(b)), features a rigid button for filling the reserved space for tactel, while the opposite side of the fixture near the base provides through-holes corresponding to the end points of each channel, facilitating the removal of air bubbles during the injecting process (Fig. 3(a)). The fixture was then clamped and secured using bolts. After that, Clear Flex 30 Part A and B were mixed at a 1:1 ratio, followed by thoroughly stirring for 5 minutes. The solution was then placed in a vacuum pump to effectively remove air bubbles. Subsequently, it was transferred to a syringe, which was placed in the vacuum pump again for further removal bubbles. Importantly, the fixture was designed with a connector that directly connects to the syringe (Fig. 3(d)), and the solution was slowly injected along an L-shaped trajectory into the mold of the sensor, allowing efficient elimination of bubbles in the solution during the bottom-up flowing process. The design of the fixture enhances the precision of fabricating the waveguides, which was particularly crucial for small-size sensor production. After cured at room temperature for 24 hours, the fixed mold was opened, allowing for the extraction of the sensor. A mixture of Dragon Skin 20 with black silicone rubber pigment was poured into the reserved space to make the soft tactel (Fig. 3(e)). Once the tactel cured, three light detecting sensors were positioned and secured in the designated slots at the end of each channel, completing the fabrication of the sensor (Fig. 3(f)).

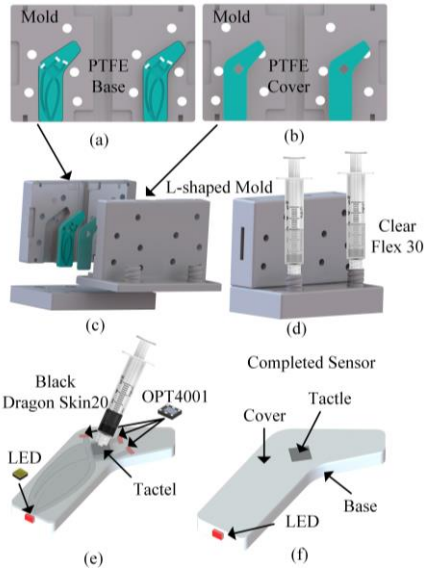

Fig. 3. Fabrication process of the optical-based sensor. (a) CNC molds of PTFE base. (b) CNC molds of PTFE cover. (c) Sealing with L-shaped fixed mold. (d) Injecting core material. (e) Injecting Dragon Skin 20 to form the tactel and assembling with the LED and light detectors. (f) The proposed sensor is completed when the tactle cured.

The completed sensor consists of following components:

- Light source: The green XQ-E High Intensity LED (CreeLED, Inc.) was chosen as the light source, emitting light that travels towards the input and then it is divided into three channels.
- Three optical waveguides: each waveguide intersect each other with 90 degrees, which was determined to minimize light loss while maximize the efficient utilization of light energy [33].
- A square soft tactile element (Tactel): was formed by the intersection of three channels and it is designed to measure the external force;
- A shell base: serving as both the cladding material and a rigid support structure for the optical waveguides;
- A shell cover: positioned atop the base to effectively shield the waveguides from external dust contamination and isolate them from the influence of ambient light.
- Three detectors: highly sensitive light sensors OPT4001 (Texas Instruments Inc.) with the dimension of 0.84mm × 1.05 mm were used as the detector and were employed at the end of each channel to measure the changing of the light intensity.

D. *Experimental Setup*

After the fabrication of the sensor, an experimental setup was built for the calibration experiments, as depicted in Fig. 4. The sensor was securely mounted on a science desk, while a 3-axis linear stage (Oumefar, LD40-LM) was installed on a linear guide (Newmark Systems Inc., ET-200-21). The angle between the applied force and the plane of the sensor could

be adjusted by rotating the linear guide. The three-axis displacement platform was utilized to control the direction of the external force. The force was then transmitted to the tactel of the sensor through a force indenter, and the magnitude of the applied force was accurately measured by a Nano 17 force sensor (Nano17-E, ATI Inc.) positioned behind the force indenter, serving as the ground truth. The output light intensity of the sensor was collected by light sensors (OPT4001) arranged at the end of each channel and transmitted to a PC via Arduino for subsequent data analysis.

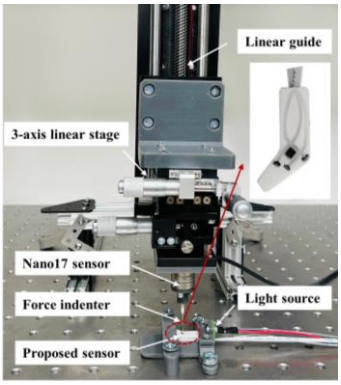

Fig. 4. Platform setup. It consists of a liner guide, a 3-axis linear stage,a Nano 17 force sensor, a force intenter, a LED light source and the proposed sensor.

It is worth emphasizing that the interaction between the indenter and the tactel involves a complex hard-soft contact deformation process. To achieve uniform deformation of the tactel, simulation analyses were conducted with both a flat indenter and a spherical indenter. The force indenters were continuously displaced towards the sensor at a fixed angle of 60 degrees, with each step of 0.1mm. Concurrently, the variations of the output light intensity were recorded and analyzed during the process. In the case of the flat indenter, as shown in Fig. 5(a), the initial contact between the indenter and the tactel resembles either point contact or line contact, thereby inducing non-uniform deformation of the tactel. Consequently, the relationship between the variation of light intensity and the step is not monotonous but exhibits fluctuations, as shown in Fig. 5(b).

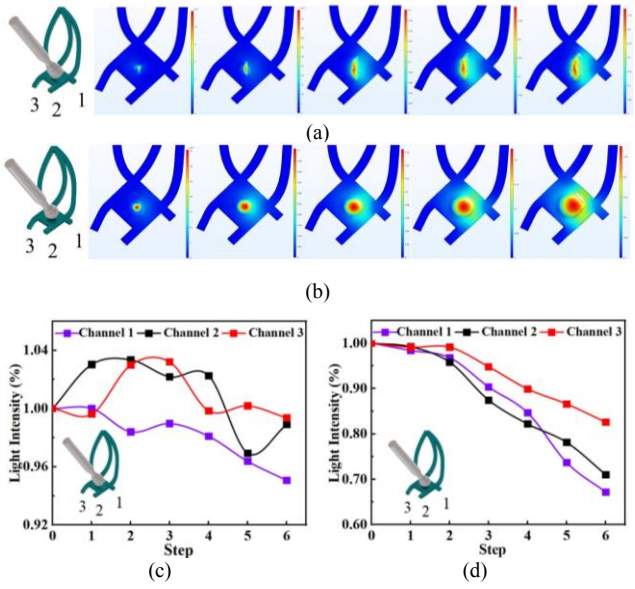

Fig. 5. The simulation results of different shapes of indenter. (a) and (b) The deformation of the tactel with a flat and a spherical indenter, respectively. (c) The relationship between the light intensity and the force applied by the flat indenter. (d) The relationship between the light intensity and the force applied by the spherical indenter.

Conversely, when employing a spherical indenter, the deformation of the tactel becomes more uniform. This is attributed to the relatively larger contact area between the indenter and the tactel, resulting in a more evenly distributed applied pressure on the tactel. Consequently, the change in light intensity exhibits a direct proportionality with the pressing steps. Therefore, in our experiment, we utilized a spherical indenter to ensure a consistent pressure distribution on the tactel during the calibration experiments.

III. Experiments and Results

To evaluate the performance of the sensor, normal force and shear force testing including the unloading and loading process were conducted. During the process, each set of experiments was repeated five times and the average values were calculated to reduce experimental errors. Meanwhile, simulation was performed following the same operation by using the optical ray tracing module in COMSOL, which served as a reference for experimental results. Subsequently, to establish the correlation between force and light intensity, a calibration matrix for the proposed sensor was calculated. Furthermore, the calibration matrix was utilized to determine the applied force based on the measured light intensity and the accuracy of the estimation was thoroughly analyzed. Finally, the sensor was mounted on surgical forceps and real-time force feedback testing was performed.

A. Normal Force Sensing

Firstly, the force indenter and the sensor were vertically aligned, with the force direction along the negative z-axis. Loading and unloading experiments were conducted to obtain the relationship between normal force and the corresponding response of the optical waveguide. The outputs of the three channels were normalized, with an initial value set at 1. As shown in Fig. 6, upon applying a normal force magnitude of 3.5N, channels 1, 2, and 3 exhibited reductions to 54.49%, 57.01%, and 64.23% of their initial value, respectively. The results demonstrate the near-linear correlation between the outputs of all three channels and the applied force, thus demonstrating the capability of the sensor to effectively measure normal forces.

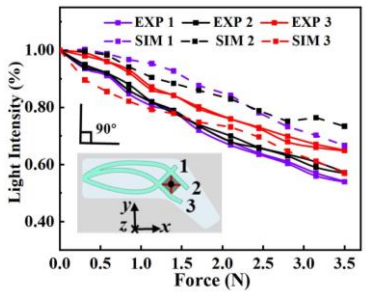

Fig. 6. Loading and unloading curves of the sensor under normal force.

B. Shear Force Sensing

During the shear force process, the linear guide and the sensor were aligned at a fixed angle of 60°, and the force

indenter was systematically pressed against the tactel in various directions along a 360-degree rotation. The corresponding outputs of the sensor were recorded and subsequently analyzed. The obtained results from experiment and simulation were depicted in Fig.7, illustrating the relationship between shear force and the respective sensor outputs. It is noteworthy that the applied force consists both normal and shear force, thereby influencing the behavior of all three channels. Specifically, an evident decreasing trend in the output responses was observed across all channels as the magnitude of the applied force increased.

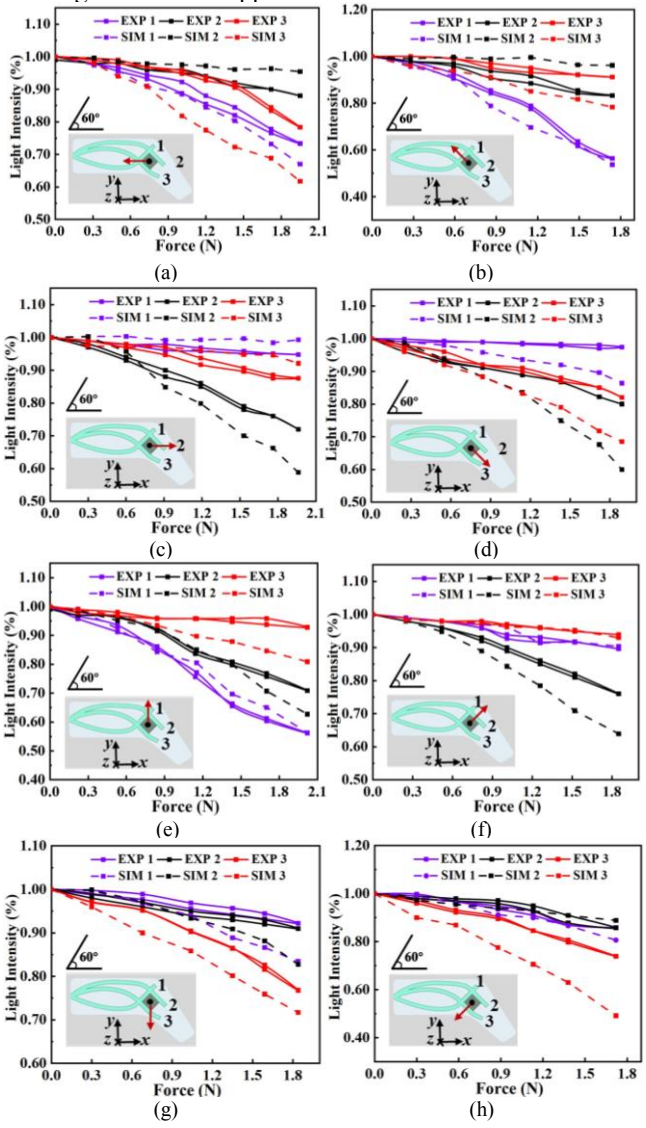

Fig. 7. The relationship between output light intensity and the force applied. Force intentor forms 60° with sensor's plane. (a) The shear force along negtive x-axis. (b) The shear force along at a 45°, formed by the negative x-axis and the positive y-axis. (c) The shear force along positive y-axis. (d) The shear force along at a 45°, formed by the positive x-axis and the positive y-axis. (e) The shear force along positive x-axis. (f) The shear force along at a 45°, formed by the positive x-axis and the negative y-axis. (g) The shear force along negative y-axis. (h) The shear force along at a 45°, formed by the negative x-axis and the positive y-axis.

Also, it can be observed that the channel responses show distinguishable patterns for different orientations. Correspondingly, within identical orientations, both experimental and simulated outcomes show analogous trends of variation while the simulation results closely conforms to linear tendencies as an idealized model. The difference between experiment results and simulation can be attributed to the influence of fabrication errors in the manufacturing process of the sensor. All subsequent analyses were based on the experimental results.

In Fig.7 (a), the application of shear force along the negative x-direction resulted in notable compression and more substantial output reduction in channels 1 and 3 compared to channel 2. Consequently, channel 1 and 3 were identified as the responsive channels for this particular direction. Conversely, Fig.7 (e) demonstrated that when the shear force was applied along the positive x-direction, channel 2 exhibited a sharp decrease reaching a reduction of 28% at a force magnitude of 1.9N, while channels 1 and 3 demonstrated relatively smaller reductions of 5.3% and 12.5%, respectively. This verified that channel 2 is the responsive channel for the negative x-direction. Similarly, the results of the force applied along the y-axis are presented in Fig.7 (c) and (g), with channel 1 and 2 corresponding to the positive y-direction, and channel 3 corresponding to the negative y-direction.

It is worth noting that due to the asymmetric design of the sensor, when the force direction formed a 45-degree angle along the positive X-direction and negative Y-direction (as shown in Fig.7 (f)), the force acted on the rigid base rather than directly on the channels. As a result, the tactel experienced lateral deformation, resulting in compression and subsequent optical loss in channel 2 and channel 3.

In summary, Fig.7 shows that the sensor demonstrates discernible output patterns in response to varying force directions, thereby enabling effective shear force detection.

C. Sensor Characterization

It is noticeable that there is inconsistency of the output intensity of the sensor during loading and unloading, which is commonly characterized as hysteresis. This hysteresis can be attributed to the softness of the sensor's material because it takes a certain time to revert to its original undeformed state. The hysteresis of the proposed sensor is calculated by (2) and (3) [21].

$$H = \frac{\Delta Y_{max}}{Y_{FS}} \times 100\% \tag{2}$$

$$\Delta Y_{max} = \left| \overline{y_{unl.i}} - \overline{y_{loa.i}} \right|_{max} \tag{3}$$

where $\overline{y_{unl.i}}$ is the average value of output light intensity during unloading; $\overline{y_{loa.i}}$ is the average value of output light intensity during loading, Y_{FS} is the full range output. The calculated results indicate that the maximum offset ΔY_{max} is 0.0369N and the average hysteresis errors for the proposed sensor is 1.23%.

Repeatability is defined as the extent of variation in the measured output light intensity when force is applied from the same direction. It can be quantified through (4):

$$R = \delta_{max} \times 100\% \tag{4}$$

where δ_{max} is the maximum value of standard deviation during loading and unloading. According to Bessel formula (5) and (6), δ_{max} can be efficiently calculated.

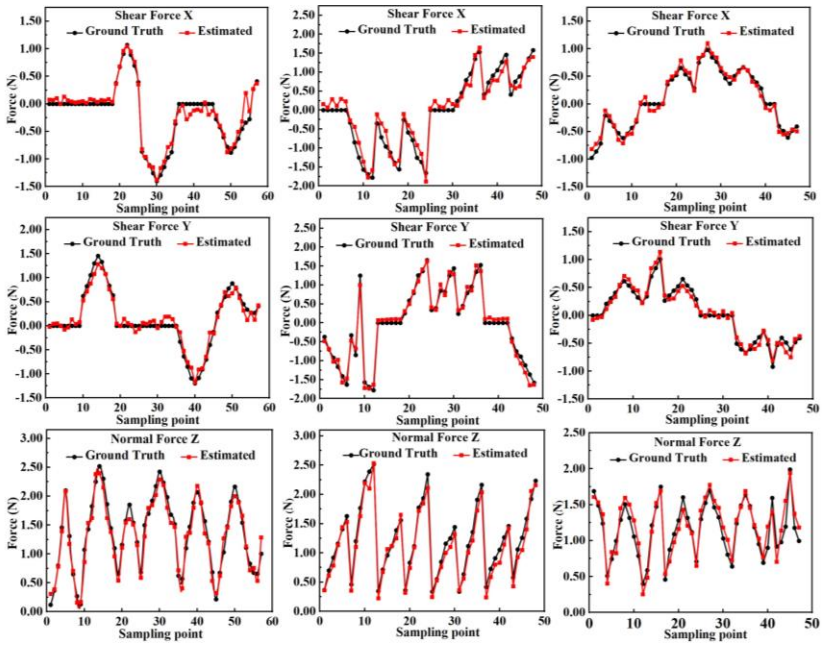

(a) 30° (b) 45° (c) 60°

Fig. 8. Comparision between the force measured by the proposed sensor and the ground truth measured by Nano17. (a) Force intentor forms 30° with sensor's plane. (b) Force intentor forms 45° with sensor's plane. (c) Force intentor forms 60° with sensor's plane.

$$\delta_{unl.i}=\sqrt{\frac{1}{n-1}\sum_{j=1}^{n}(y_{unli.j}-\overline{y_{unl.i}})^{2}} \tag{5}$$

$$\delta_{loa.i}=\sqrt{\frac{1}{n-1}\sum_{j=1}^{n}(y_{loa.ij}-\overline{y_{loa.i}})^{2}} \tag{6}$$

where n is the number of trials, and n=725 in this paper. R for three channels of the proposed sensor are 0.697%, 0.569%, and 0.798%, respectively, which show good repeatability.

D. Sensor Calibration Matrix

The calibration matrix C was utilized to quantitatively characterize the relationship between force and light intensity, as depicted in (7), where O and F represent the outputs of the three channels and the magnitudes of the three-axis forces, while n represents the number of samples, and n=725 in this paper. Based on the experimental results, C can be calculated using (8).

$$[O]_{3\times n}=[C]_{3\times 3}\cdot[F]_{3\times n} \tag{7}$$

$$[C]_{3\times 3}=[O]_{3\times n}\cdot[F]^{-1}_{3\times n} \tag{8}$$

$$\text{where}\ [C]_{3\times 3}=\begin{bmatrix}0.16490 & -0.0996 & 0.6674\\ -0.0897 & -0.0045 & 0.6808\\ 0.00047 & 0.1283 & 0.7110\end{bmatrix}$$

Therefore, the applied forces can be inferred according the calibration matrix and the measured light intensity outputs, as shown in (9), which constitutes the underlying principle of the force feedback of this sensor.

$$[F]_{3\times 1}=[C]^{-1}_{3\times 3}\cdot[O]_{3\times 1} \tag{9}$$

$$\text{where}\ F_{3\times 1}=\begin{bmatrix}F_x\\F_y\\F_z\end{bmatrix}, O_{3\times 1}=\begin{bmatrix}O_1\\O_2\\O_3\end{bmatrix}.$$

To validate the feasibility of the calibration matrix, the experimental setup was adjusted to angles of 30°, 45°, and 60° and forces were applied in various directions. The estimated forces, obtained using Equation 3, were compared with the forces measured by the Nano17 sensor to assess the accuracy of the sensor. The results and the corresponding average error are presented in Fig.8 and Table 2 respectively. It can be observed that for the proposed sensor, the average amplitude error is 0.089N, the vector's angle error is 6.96°, indicating a high level of consistency with the ground truth. This corroborates the practicality and high precision of the calibration matrix for forces estimation.

TABLE II. THE ERROR OF THE PROPOSED SENSOR

Included Angle	Average Error	
	Amplitude Error (N)	*Angle Error(°)*
30°	0.0833	6.7012
45°	0.0962	8.2293
60°	0.0879	4.964

E. Testing With a Sensorized Surgical Forceps

To validate the sensor's performance integrated into the surgical instruments, a prototype of surgical forceps incorporating the proposed sensor was designed, as shown in Fig.1 and Fig. 9. The proposed sensor was installed on the one side of the jaw, while the LED was embedded at the rear end of the opposite side the jaw. Significantly, based on the simulation results of the hard-soft contact deformation, a spherical force indenter integrated with the cover was designed and positioned on the top of the tactel as the force transmitter to guarantee uniform deformation during the experimental procedure, shown in Fig. 9(b). The lower surface of the cover consists of four pillars, each situated at the corners and measuring 0.5mm in height, along with a

spherical force indenter of the same height in the center. In initial state, the lower surface of the indenter makes direct contact with tactel. The pillars provides the indenter with downward mobility and also separate the remaining sections of the cover from the tactel. When the forceps are closed, the clamped object applies downward force to the force indenter, causing it to compress the tactel. Subsequently, the tactel squeezes on lateral sides of the optical fiber channel, leading to the deformation of waveguides. Consequently, the force is transmitted from the surface of the cover to the optical fiber channels via tactel.The signal wires were routed through the back of the sensor and passed through the shaft of the forceps to the end, as shown in Fig.9 (c) and Fig. 9(d).

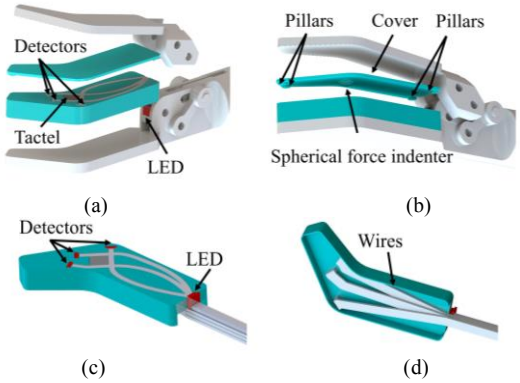

Fig. 9. The integrated forcep. (a) Assembled sensorized forceps. (b) 3D model of gripper. (c) The signal wires passed through the shaft of the forceps to the end. (d) The wires were routed through the back of the sensor.

The utilization of forceps in MIS can be categorized into two main scenarios: grasping and pulling. Grasping primarily involves the application of normal forces, while pulling predominantly entails the application of shear forces. To simulate vascular conditions during surgery procedures, a rubber tube filled with water under certain pressure was selected as the demonstration model for the verification of the integrated system. The validation experiments were conducted in two groups. Firstly, the forceps performed a grasping motion on the tube, followed by the pulling motion along the positive and negative y-axis. Subsequently, the forceps grasped the tube and moved it along positive and negative x-axis directions, thereby evaluating the detection of forces in different directions. Data collection was conducted during this process at a sampling frequency of 5 Hz, and the obtained three-axis force value are presented in Fig.10.

It is important to highlight that when the forceps gradually grasp the tube, both shear and normal forces are simultaneously generated. This phenomenon arises due to the application of a perpendicular force on the surface of the tube, resulting in the decomposition of the force into components of normal and shear forces, as shown in Fig. 11.

In summary, the results presented above demonstrate that the forceps accurately detected the grasping and pulling processes, allowing for precise identification of force magnitude and direction. These outcomes indicate the sensor's capability to provide real-time force feedback, validating its effectiveness and reliability.

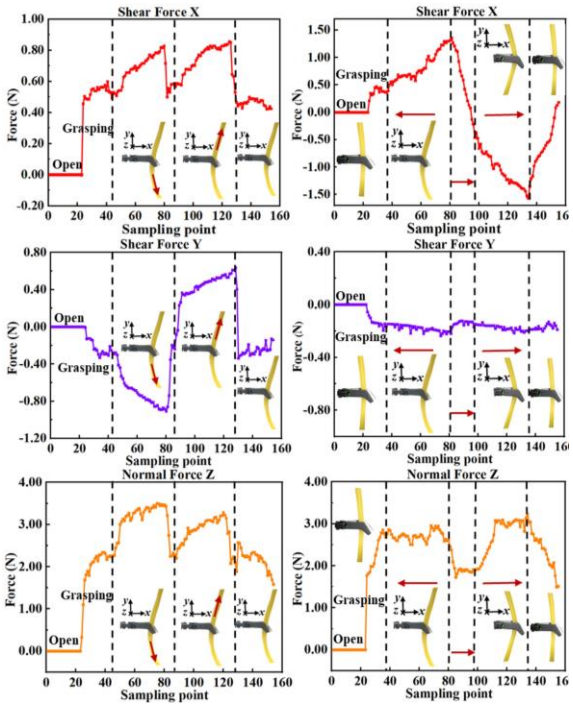

Fig. 10. Responses of the integrated force sensor.(a) Grasping and pulling processes along y direction. (b) Grasping and pulling processes along x direction.

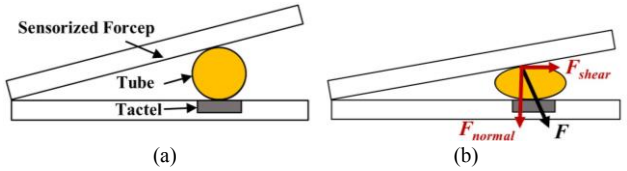

Fig. 11. The force applied on the rubber tube filled with water. (a) Original status. (b) Grasping motion generates both the shear and normal forces.

IV. CONCLUSION AND DISCUSSION

This paper presents an integrated and a novel 3-Axial force sensor designed to provide real-time force feedback for surgical forceps in MIS. The sensor consists of three intersecting optical waveguides, forming a square sensing area of 2.6mm, which enables the precise measurement of both the magnitude and direction of applied forces. The propagation of light within the waveguides follows the principle of total internal reflection (TIR) while it is disrupted when external forces applied, resulting in the light loss. The relationship between force magnitude and output light intensity was established accordingly, while the tactile undergoes asymmetric deformation in response to forces applied from different directions. As a result, the three waveguides generate distinct output patterns, which enable the determination of force direction.

To validate the working principle and investigate the impact of force indenter's shapes on the contact deformation of soft-rigid interfaces, simulations were conducted using COMSOL. And calibration experiments were conducted for both normal and shear force sensing. A calibration matrix was established to determine the correlation between 3D forces and light intensities. The estimated forces were

compared with ground truth, demonstrating the sensor's capability to accurately measure forces ranging from 0 to 3N with the average amplitude error 0.089N. Furthermore, the compact light source circuit and detection circuit were integrated into a prototype of surgical forceps and subsequently to perform experiments involving grasping and pulling. The experimental results validate the sensor's effectiveness in providing force feedback for the tasks in MIS, thus validating the promising feasibility of its practical application in surgical forceps.

In future work, we will further focus on optimizing and minimizing the sensor design to enhance its versatility and broaden its potential applications in MIS. Additionally, animal clinical trials will be conducted to assess the feasibility and effectiveness of the sensor in a clinical environment.

APPENDIX

The videos demonstrate the response of the integrated sensor during grasping and pulling process.

REFERENCES

[1] B. Jaffray, "Minimally invasive surgery," *Arch Dis Child*, vol. 90, no. 5, pp. 537–542, May 2005.

[2] P. Puangmali, K. Althoefer, L. D. Seneviratne, D. Murphy, and P. Dasgupta, "State-of-the-art in force and tactile sensing for minimally invasive surgery," *IEEE Sens J*, vol. 8, no. 4, pp. 371–380, Apr. 2008.

[3] E. P. W. van der Putten, R. H. M. Goossens, J. J. Jakimowicz, and J. Dankelman, "Haptics in minimally invasive surgery – a review," *Minimally Invasive Therapy & Allied Technologies*, vol. 17, no. 1, pp. 3–16, 2009.

[4] G. Tholey, J. P. Desai, and A. E. Castellanos, "Force Feedback Plays a Significant Role in Minimally Invasive Surgery: Results and Analysis," *Ann Surg*, vol. 241, no. 1, p. 102, Jan. 2005.

[5] A. M. Okamura, "Haptic Feedback in Robot-Assisted Minimally Invasive Surgery," *Curr Opin Urol*, vol. 19, no. 1, p. 102, Jan. 2009.

[6] S. S. Sastry, M. Cohn, and F. Tendick, "Milli-robotics for remote, minimally invasive surgery," *Rob Auton Syst*, vol. 21, no. 3, pp. 305–316, Sep. 1997.

[7] W. Othman *et al.*, "Tactile Sensing for Minimally Invasive Surgery: Conventional Methods and Potential Emerging Tactile Technologies," *Front Robot AI*, vol. 8, p. 705662, Jan. 2022.

[8] Y. Al-Handarish *et al.*, "A Survey of Tactile-Sensing Systems and Their Applications in Biomedical Engineering," *Advances in Materials Science and Engineering*, vol. 2020, 2020.

[9] A. SONG and L. FU, "Multi-dimensional force sensor for haptic interaction: a review," *Virtual Reality & Intelligent Hardware*, vol. 1, no. 2, pp. 121–135, Apr. 2019.

[10] Y. Wei and Q. Xu, "An overview of micro-force sensing techniques," *Sens Actuators A Phys*, vol. 234, pp. 359–374, Oct. 2015.

[11] Y. Yang, M. Zhao, H. Yinguo, H. Zhang, N. Guo, and Y. Zheng, "Micro-force sensing techniques and traceable reference forces: a review," *Meas Sci Technol*, vol. 33, no. 11, p. 114010, Aug. 2022.

[12] J. Rado *et al.*, "3D force sensors for laparoscopic surgery tool," *Symposium on Design, Test, Integration and Packaging of MEMS/MOEMS, DTIP 2016*, Jul. 2016.

[13] C. Hou *et al.*, "A Sensorised Forcep Based on Piezoresistive Force Sensor for Robotic-assisted Minimally Invasive Surgery" *Proceedings of the 16th Annual IEEE International Conference on Nano/Micro Engineered and Molecular Systems*, NEMS 2021, pp. 60–63, Apr. 2021.

[14] F. Ju *et al.*, "A miniature piezoelectric spiral tactile sensor for tissue hardness palpation with catheter robot in minimally invasive surgery," *Smart Mater Struct*, vol. 28, no. 2, p. 025033, Jan. 2019.

[15] S. Sharma, R. Aguilera, J. Y. Rao, and J. K. Gimzewski, "Piezoelectric needle sensor reveals mechanical heterogeneity in human thyroid tissue lesions," *Scientific Reports* 2019 9:1, vol. 9, no. 1, pp. 1–9, Jun. 2019.

[16] C. H. Chuang, T. H. Li, I. C. Chou, and Y. J. Teng, "Piezoelectric tactile sensor for submucosal tumor detection in endoscopy," *Sens Actuators A Phys*, vol. 244, pp. 299–309, Jun. 2016.

[17] O. H. Paydar *et al.*, "Fabrication of a thin-film capacitive force sensor array for tactile feedback in robotic surgery," *Proceedings of the Annual International Conference of the IEEE Engineering in Medicine and Biology Society*, *EMBS*, pp. 2355–2358, 2012.

[18] U. Kim, D. H. Lee, W. J. Yoon, B. Hannaford, and H. R. Choi, "Force Sensor Integrated Surgical Forceps for Minimally Invasive Robotic Surgery," *IEEE Transactions on Robotics*, vol. 31, no. 5, pp. 1214–1224, Oct. 2015.

[19] U. Kim, Y. B. Kim, D. Y. Seok, J. So, and H. R. Choi, "A surgical palpation probe with 6-axis force/torque sensing capability for minimally invasive surgery," *IEEE Transactions on Industrial Electronics*, vol. 65, no. 3, pp. 2755–2765, Mar. 2018.

[20] N. Bandari, J. Dargahi, and M. Packirisamy, "Tactile sensors for minimally invasive surgery: A review of the state-of-the-art, applications, and perspectives," *IEEE Access*, vol. 8, pp. 7682–7708, 2020.

[21] Y. Li, J. Hu, D. Cao, S. Wang, P. Dasgupta, and H. Liu, "Optical-Waveguide Based Tactile Sensing for Surgical Instruments of Minimally Invasive Surgery," *Front Robot AI*, vol. 8, p. 773166, Jan. 2022.

[22] H. Xie, H. Liu, L. D. Seneviratne, and K. Althoefer, "An optical tactile array probe head for tissue palpation during minimally invasive surgery," *IEEE Sens J*, vol. 14, no. 9, pp. 3283–3291, 2014.

[23] B. Kuebler, U. Seibold, and G. Hirzinger,, "Development of actuated and sensor integrated forceps for minimally invasive robotic surger," *The International Journal of Medical Robotics and Computer Assisted Surgery*, vol. 1, no. 3, pp. 96–107, Sep. 2005.

[24] Stolov, A. A et al., "Sterilization Effects on Optical Fibers for Clinical Use" *BioPhotonics*, Sep. 2015.

[25] H. Bai, S. Li, J. Barreiros, Y. Tu, C. R. Pollock, and R. F. Shepherd, "Stretchable distributed fiber-optic sensors," *Science* (1979), vol. 370, no. 6518, pp. 848–852, Nov. 2020.

[26] J. Back, P. Dasgupta, L. Seneviratne, K. Althoefer, and H. Liu, "Feasibility study- novel optical soft tactile array sensing for minimally invasive surgery," *IEEE International Conference on Intelligent Robots and Systems*, vol. 2015-December, pp. 1528–1533, Dec. 2015.

[27] Y. Tang *et al.*, "Optical Micro/Nanofiber-Enabled Compact Tactile Sensor for Hardness Discrimination," *ACS Appl Mater Interfaces*, vol. 13, no. 3, pp. 4560–4566, Jan. 2021.

[28] S. C. Lim, H. K. Lee, and J. Park, "Grip force measurement of forceps with fibre Bragg grating sensors," *Electron Lett*, vol. 50, no. 10, pp. 733–735, May 2014.

[29] X. He, J. Handa, P. Gehlbach, R. Taylor, and I. Iordachita, "A submillimetric 3-DOF force sensing instrument with integrated fiber bragg grating for retinal microsurgery," *IEEE Trans Biomed Eng*, vol. 61, no. 2, pp. 522–534, Feb. 2014.

[30] T. Li, C. Shi, and H. Ren, "A High-Sensitivity Tactile Sensor Array Based on Fiber Bragg Grating Sensing for Tissue Palpation in Minimally Invasive Surgery," *IEEE/ASME Transactions on Mechatronics*, vol. 23, no. 5, pp. 2306–2315, Oct. 2018.

[31] J. Hu, D. Cao, Y. Li, and H. Liu, "Polymer-Based Optical Waveguide Tactile Sensing Method for 3-D Surfaces," *IEEE Sens J*, vol. 23, no. 8, pp. 8761–8768, Apr. 2023.

[32] F. De Chiara, J. Hu, S. Wang, R. Wang, and H. Liu, "Design of optical waveguide channels for 3D distributed tactile sensing," *Proceedings of IEEE Sensors*, vol. 2021-October, 2021.

[33] D. Cao, J. Hu, Y. Li, S. Wang, and H. Liu, "Polymer-Based Optical Waveguide Triaxial Tactile Sensing for 3-Dimensional Curved Shell," *IEEE Robot Autom Lett*, vol. 7, no. 2, pp. 3443–3450, Apr. 2022.

[34] M. Gauch, M. Ließmann, H. Ehlers, and D. Ristau, "Optical properties of fluorocarbon thin films prepared by ion beam sputtering of PTFE," *Optical Interference Coatings (2013), paper ThA.2,* p. ThA.2, Jun. 2013.